DRAG ELEMENTS OF INDOOR MODELS

Raymond B. Harlan

INTRODUCTION

Although quite a bit of drag data for indoor models has been presented in the literature (1 to 4), much of it is not commonly known and is difficult to obtain. None of the authors calculates the drag of individual model components. This paper attempts to do so in order for the modeler to develop a better perspective of the characteristics of drag that limit a model's performance. The work has been greatly facilitated by the well-known volume by Hoerner, **Fluid-Dynamic Drag** (5) which is almost everything you ever wanted to know about drag. The analytic treatment has been supplemented by glide tests of a 65cm FAI model representative of current design trends.

McBrides' tests (1) were performed in a wind tunnel in which the wings had spans of 70 percent of the test section width and an aspect ratio of 3.44. The data given probably represent a somewhat distorted measure of the three dimensional lift and drag characteristics of wings since the tips were near, but did not touch, the tunnel walls. The Reynolds number was 12,800, in the correct range for indoor models. His minimum drag coefficients ranged from .008 to .022, depending upon the airfoil. These are considerably lower than those measured in the present tests. Hacklinger (4) showed minimum drag coefficients for a complete model near .075 which correlates well with these tests. Schmitz (3) tested a Goetttingen 417a curved plate wing and, after subtracting drag due to lift, found a profile drag of .027 at a Reynolds number of 21,000. This corresponds closely to values of skin friction drag calculated in this paper, if some account is taken of the pressure drag due to the slightly blunt leading of the three percent thick plate. The JAL (Jordan-Traveller Junior Aviation League, Boston, Mass.) tests examined a series of eight percent thick wings with rectangular planform of aspect ratio six(2). Minimum drag coefficients ranged between .06 and .075 for the series of airfoils with high points between ten and sixty percent chord. Many other tests were made, including the effects of spar placement, spar fairing, and wing-fuselage interference. Tunnel speed was 3.1 feet per second.

For the uninitated, the drag coefficient is a nondimensional description of the resistance of a body to move through the air. It is nothing more than the drag force divided by the dynamic pressure (q) and some reference area. The dynamic pressure is half the density of air times the square of the air velocity. Multiplying it by an area results in a product with the dimensions of force, hence the drag coefficient is dimensionless.

$$C_D = D/qS$$

$$q = \rho V^2/2$$

The drag coefficient normally is separated into two parts, one due to the air having to be pushed out of the way by the body flying through it and one due to the characteristics of the lift distribution on the wing. The first (CDo) is relatively constant, varying only with velocity as a result of changing flow conditions determined by the interplay of viscosity and inertia of the air particles (Reynolds number effects). It is called profile or parasite drag. The drag due to lift varies considerably with angle of attack.

Drag coefficients of parts of the model are based on either the frontal area of the part, and are denoted CDo, or on the surface area of the wing, denoted by CD. Many of these coefficients are functions of Reynolds numbers which is a ratio of the inertia forces of the moving air particles to their viscous forces. At low speeds, viscous forces predominate and Reynolds numbers are correspondingly low. This ratio is expressed as a function of speed, length, and kinematic viscosity. The length can be either the distance (L) the air particles move over the body (e.g., chord) or, for spars, a diameter or depth (d). A useful form of Reynolds number is,

$$R_L = 534VL$$

V in ft/sec, L in inches

All of the calculations and measurements presented relate to the 65cm FAI class model shown in Figure 1. This model weighed 1.14 grams, including a substitute weight for the propeller. For the glide tests, the model was trimmed for the normal near-stall condition required for best endurance. With a 1.4 gram motor, the center of gravity was located at 75 percent of the root chord.

PROFILE DRAG

Surface Skin Friction

The flow over the flying surfaces is entirely laminar in the Reynolds number region for indoor models. As a result, the most important contributor to the drag of a model (the skin friction) can be very simply expressed. For Reynolds numbers about 1000, it is given in coefficient form by (5),

$$C_f = 1.328/\sqrt{R_L}$$

FIGURE 1 TEST MODEL PLANFORM

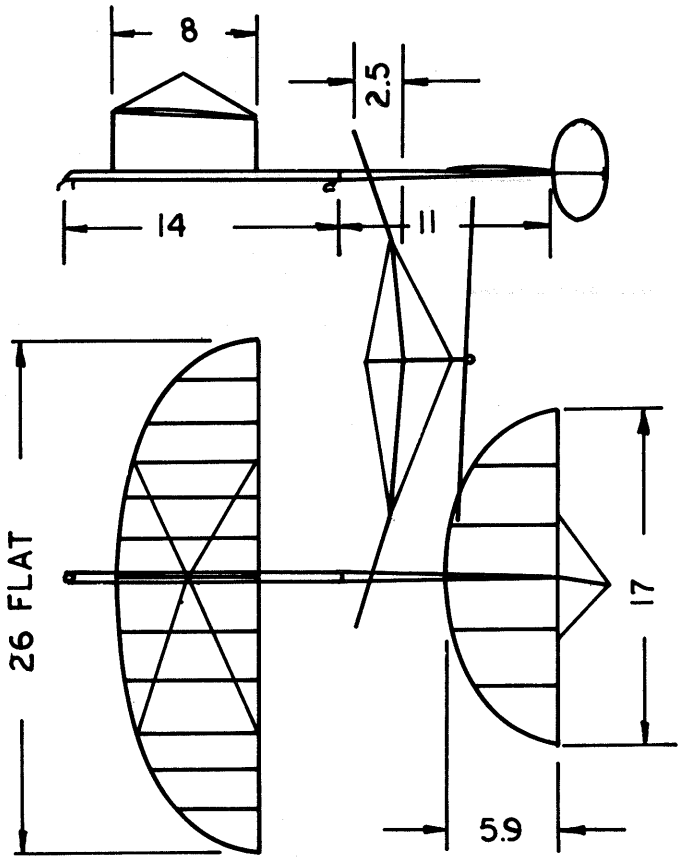

The corresponding drag coefficient is twice this value, since Cf represents the friction due to flow over one surface. The Reynolds number can be based on average chords which are 6.66", 4.88" and 2.08" for the wing stabilizer and rudder, respectively. The result is a drag coefficient for the wing ranging between .032 and .020 in the speed range of 2 to 5 feet per second.

As with all drag coefficient components, except for the wing friction drag which is properly scaled, the stabilizer and rudder friction drag coefficients must be rescaled to reflect using the wing area to normalize drag elements to obtain drag coefficients. For instance, for the stabilizer,

$$C_D = 2.656 S_t / S\sqrt{R_L}$$

where RL is based on the average stabilizer chord. The result is a coefficient ranging between .018 and .011 for the aforementioned speed range. These values are shown in Figure 2 which compares all drag coefficient elements. The total skin friction drag is over 2.7 times the remainder of the profile drag at the lowest speed.

Spar Pressure Drag

Behind rectangular wing spars are found partially developed vortex systems resulting from flow separation from the rear side. Because of the microfilm skin attached to the upper surface of the spar, it is extremely difficult to estimate the degree of vortex development and, consequently, the pressure drag due to the mixing of this flow. No good experimental data exists for such a configuration in the Reynolds number region of interest. Fortunately one phenomenon aids in reducing the importance of spar pressure drag. The boundary layer is so thick at the trailing edge of any of the flying surfaces that there literally is no flow around the trailing edge spars. For laminar flow, the boundary layer thickness is given by(5),

$$\delta/L = 5.5/\sqrt{R_L}$$

Thus, for an eight inch chord at 2 ft/sec, δ = .47 inches.

To gain an appreciation of the effects of rectangular spars and surface skins emanating from them, it is useful to examine the existing data, despite the inappropriate Reynolds of 10^4 to 10^5 based on frontal area. A square spar has about twice the drag coefficient of a round spar if no skins are attached (5, pp. 3-17). Circular spars with "Splitter plates" on the centers of their trailing sides (O———) yield drag coefficients about 63% of the lone round spar. These plates effectively prevent full wake mixing which produces a lot of drag. One might expect the combination of a square spar and an upper surface skin to yield a drag coefficient which is greater than that for a lone round spar by the product of the factors in these two examples (2 x .63 = 1.26). However, indoor model spars have Reynolds numbers less than 100 and the vortex system probably is much less fully developed, even though the spars have sharp edges. Consequently, the drag may be substantially less. An excellent picture of the development of vortices with increasing Reynolds number is shown in (6, p. 553).

A simple experiment was undertaken to identify the spar drag at the proper Reynolds number. A .04" x .04" x 12" balsa spar was dropped and timed over a seven foot fall. From this, a drag coefficient, based on frontal area, of 1.53 was calculated for a speed of 3.87 ft/sec. A .75" microfilm "splitter plate" was attached to the spar and the tests were repeated. Then the drag coefficient of the spar became .61, a marked change. Finally, the film was removed and the spar was rounded and again dropped. The drag coefficient was 1.07. This experiment suggests that the spar drag is about .57 that of a lone round spar. However, experimental uncertainties lead to a large uncertainty in the drag of the square spar with the skin attached, since most of its measured drag was due to skin

friction which was estimated by equation (4) and subtracted. To be on the conservative side, it is assumed that the spar pressure drag is 65 percent of that for a lone round spar having the same frontal area. In the Reynolds number region of interest, this drag coefficient can be expressed by

$$C_{D_\bullet} = 1.21 - 3.33 \times 10^{-3} R_d$$

It should be noted that, while this formula is not well substantiated, if the drag of a rectangular spar is taken to be larger (1.26x) than the round spar, as the high Reynolds number indicates, the total profile drag coefficient is increased only 15 percent.

Values for wing and stabilizer leading edge spar pressure drag coefficients, based on wing area, S, are about one-fifth the corresponding skin friction coefficients.

One more type of spar pressure drag should be included. The wing stilts are circular cylinders also working at Reynolds numbers near 100. Their drag coefficients can be determined directly from data given by (5, pp. 3-9). An analytic expression is assumed to be

$$C_{D_\bullet} = 3\, R_d^{-1/7}$$

Values for this, based on wing area, are shown in Figure 2.

FIGURE 2 DRAG COEFFICIENTS

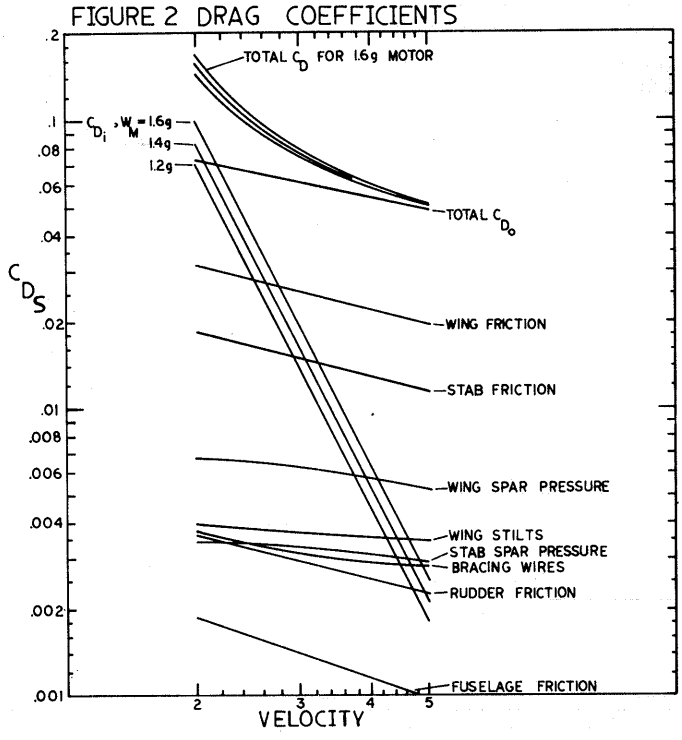

Drag of Bracing Wires

Reynolds numbers for bracing wires range from 1 to 3. At these extremely low values, there is no flow separation near the trailing side of the wire, and a simple expression for drag coefficient has been derived (5, p. 3-2),

$$C_{D_\bullet} = (10.9/R_d)/(.87 - \log R_d)$$

This yields values near 10. When normalized to the reference wing area, they are about .003. For the test FAI model, for which the top bracing wires are not perpendicular to the flow, the formula must be multiplied by $\sin^3 \alpha$, where α is the angle between the flight path and the wire. The resulting values are shown in Figure 2. The wires contribute about as much drag as the wing stilts or the stabilizer spar, or less than five percent of the total profile drag.

Fuselage Skin Friction

To simplify the analysis, it is assumed the fuselage has no angle of attack. The skin friction of an axial cylinder is increased over that of a flat plate with the same area because the boundary layer is thicker. For a laminar boundary layer, the increase in the friction coefficient above that for the flat plate is approximately (5, p. 2-7),

$$\Delta C_f = 2/R_d = 2(L/d)/R_L$$

This would be added to a coefficient calculated from equation (4). At two ft/sec, the increase amounts to nearly 100 percent for the FAI model. Values, normalized to the reference wing area and shown in Figure 2, demonstrate that this drag is nearly insignificant. It is twice as great as the rudder spar pressure drag or the cabane strut drag which are ignored.

Summary of the Profile Drag Coefficient

Included in Figure 2 is the total profile drag coefficient found by adding the individual components. It is very nearly a straight line due to the strong influence of the skin friction coefficient which is proportional to $1/\sqrt{RL}$. There is a slight shift in slope because spar pressure drag coefficients do not diminish as rapidly with increasing speed. If a straight line is assumed, the total profile drag coefficient for this FAI model is given by

$$C_{D_o} = .0986V^{-.436}$$

Drag Due to Lift

In full scale aircraft, the most important element of drag results from the way lift is distributed across the span of the wing. For indoor models it is much less important because skin friction is so great. Nevertheless, it cannot be neglected and would dominate at speeds below two ft/sec.

Any number of aerodynamics texts describe induced drag (5, 7, 8) and a serious modeler should understand its origin. Analytically, it is expressed compactly in terms of lift coefficient and aspect ratio,

$$C_{D_i} = \frac{C_L^2}{\pi A}$$

if the lift distribution is elliptical. Rarely is this the case, however, and it is normal to incorporate correction factors dependent upon planform shape. Account also must be taken of wing twist. Because of the complexity of determining these factors for an actual model, this paper assumes the induced drag coefficient to be given by the simple formula (12) but recognizes that it represents the minimum achievable.

In equilibrium flight at low glide path angles, the lift equals the weight and

$$C_L = W/qS$$

This can be applied to the test model for various weights (e.g., different motors) and in turn used in equation (12) to determine the induced drag coefficient. This coefficient is inversely proportional to the fourth power of speed and is insignificant at the higher velocities shown in Figure 2.

Because of the span limitation of FAI indoor models, an interesting characteristic of induced drag exists. By use of equation (13), this drag can be expressed as

$$D_i = W^2/\pi q b^2$$

The induced drag is dependent upon the span rather than area. Thus, for a fixed chord distribution, the induced drag is not changed by scaling up the chord. This probably was a very significant factor in the evolution of our wide chord models following the inception of the one-gram rule.

EXPERIMENTAL RESULTS

The model described in the Introduction was glide tested to determine drag and lift coefficients for various motor weights and center of gravity locations. A Polaroid camera recorded multiple flash images of the model's trajectory, Figure 3. The interval between flashes was one-half second and a scale beneath the flight path, marked in half-foot dimensions, aided accurate speed measurements. A plumb bob identified the vertical for glide path angle measurements.

FIGURE 3 GLIDE TESTS

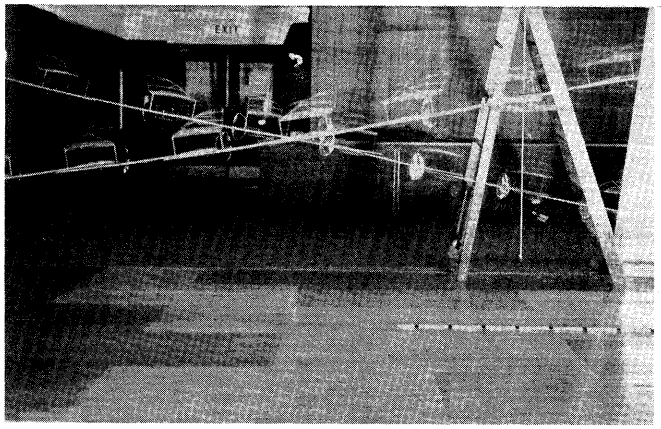

Despite the fact that tests were conducted in an unheated room and motion of people was kept at a minimum, significant scatter is present in the reduced data. Images suggest the present of some phugoid oscillation of the model, due to imperfect launch conditions. This affects speed measurements for the most part. As a result, speed was determined by measuring the time spent traversing a horizontal distance of ten feet. Curvature of the flight path, in a vertical plane, limited the accuracy of measuring flight path angle. Since the lift to drag ratio is equal to the

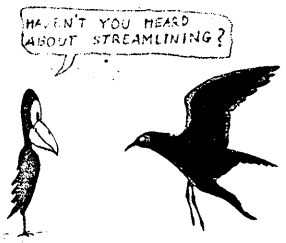

tangent of this angle, measurement uncertainties directly reflect in drag coefficient errors. Nearly all error in the lift coefficient is attributable to uncertainties in speed. The governing equations are

$$L = W \cos\gamma$$

$$D = W \sin\gamma$$

$$D/L = \tan\gamma$$

The experimental data are presented in Figure 4, together with analytic curves for profile and induced drag coefficients derived from Figure 2. At the lowest lift coefficients (or highest speeds) there is a large spread and all data exceed analytic prediction. Distortion of the wing and stabilizer, imposed by the severe flight loads at these speeds, probably accounts for the bulk of this disparity. Hacklinger (4) presents similar data showing an increase in profile drag at very low lift coefficients. Because the elasticity, it is not meaningful to measure indoor model drag under these conditions.

At higher lift coefficients, considerable scatter also is present, albeit about the analytic curves. Without resorting to curve fitting techniques, it is clear that a ten percent increase in the estimate of profile drag coefficient would place the curves near the middle of the data except at the very low lift coefficients. Because of the fairly narrow range of lift coefficients explored, it is not possible to distinguish profile and induced drag modeling errors. Without more extensive testing, individual drag component estimates cannot be improved.

CONCLUSIONS AND RECOMMENDATIONS

Drag of each component of an FAI indoor model has been analyzed and glide tests of a model have been used to support the analysis. Skin friction is the greatest single drag element at normal flight speeds. It is more than 2.6 times greater than the remainder of the profile drag. The second largest contributor to profile drag is due to the pressure distribution around spars (including wing stilts) which produces twenty percent. The drag of the bracing wires comprises only 4.6 percent of the profile drag and only 3.3 percent of the total drag at 2.5 ft/sec. At this flight speed, profile drag is nearly twice as large as the induced drag.

These results suggest the possibility of adding bracing while reducing spar depths to obtain some improvement in model drag. Such attempts were employed by West Coast modellers in the fifties with picket fence bracing. Besides being time consuming to build, spar warping due to changes in humidity eventually led to the return to simpler bracing. However, one should not hesitate to add special bracing to a wing or stabilizer to help out a particularly weak spar.

FIGURE 4 LIFT VS. DRAG

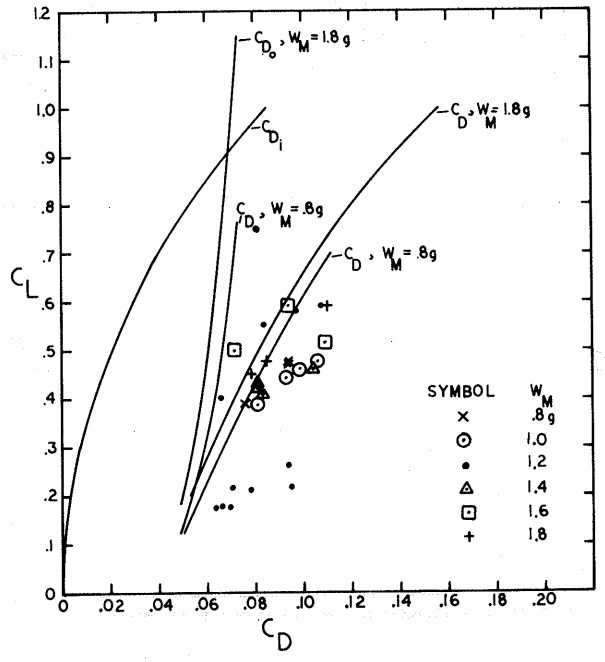

Additional experiments should be undertaken to better define spar pressure drag for the configuration and Reynolds numbers appropriate to indoor models. Drag for a greater range of lift coefficients than was tested should be explored, with emphasis on the high values at low speeds to improve the analytical model of induced drag coefficient.

Glide testing to determine lift and drag coefficients is difficult because of unsteady motion of the gliding model. The only practical way to obtain consistent data is with a good low speed wind tunnel complemented with adequate instrumentation to accurately determine air speeds and the very low force levels encountered by our models.

ACKNOWLEDGEMENTS

The author wishes to thank Mr. Curt Thiem and Mr. Tom Polgar for their assistance in conducting the model glide tests.

REFERENCES

1. McBride, J.W., "Some Technical Notes on the Present Indoor Airfoil," in Junior Aeronautics Year Book, F. Zaic, ed., 1934.
2. Journal of International Aeromodeling, Vol. 1 No. 1, Apr. 1939 and Vol. 1, No. 2, July 1939. Editors Bruno P. Marshi and Wilbur F. Tyler, Research Consultants; Herbert K. Weiss and W. Hewitt Phillips.
3. Schmitz, F. W. "Aerodynamics of Model Airplanes," PT. 1 – Airfoil Measurements. Available through National Technical Information Service, 5285 Port Royal Road Springfield, Va. 22151. Assession No. N-70-39001. Price $6.00.

4. Hacklinger, M. "Theoretical and Experimental Investigation of Indoor Flying Models." Journal of the Royal Aeronautical Society Vol. 68, Nov. 64.

5. Hoerner, S. F. "Fluid Dynamic Drag. Published by the Author, Greenbrier, 2 King Lane, Bricktown, N. J. 08723, 1965.

6. Goldstein, S. Modern Developments in Fluid Dynamics. Vol. 3, Dover Publications, Inc., New York, N.Y., 1965.

7. Perkins, C. D., and Hage, R. E., "Airplane Performance, Stability, and Control. John Wiley and Sons, Inc., New York, N.Y., 1949.

8. Abott, I. H., and Von Doenhoff, A. E., "Theory of Wing Sections. Dover Publications, Inc. New York, N.Y., 1959.

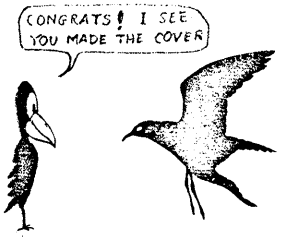

SYMBOLS

A	Aspect ratio, b^2/S	
b	Wingspan ft	ft.
C_D	Drag coefficient, D/qS	
C_{D_o}	Profile drag coefficient	
$C_{D_\bullet}$	Drag coefficient based on frontal area of a model part.	
C_{D_i}	Induced drag coefficient	
C_f	Skin friction coefficient, based on wetted area	
C_L	Lift coefficient, L/qS	
D	Drag	lbs.
L	Lift, or length upon which Reynolds number is based	lbs.or ft.
q	Dynamic pressure, $\rho V^2/2$	lb/ft^2
R_L	Reynolds number based on length of air flow over surface	
R_d	Reynolds number based on spar depth or diameter	
S	Wing area	$ft.^2$
S_t	Stabilizer area	$ft.^2$
V	Speed of the model	ft/sec
W	Weight of the model	lb.
δ	Thickness of boundary layer	ft
γ	Flight path angle	
ρ	Density of air, .00238	$slugs/ft.^3$

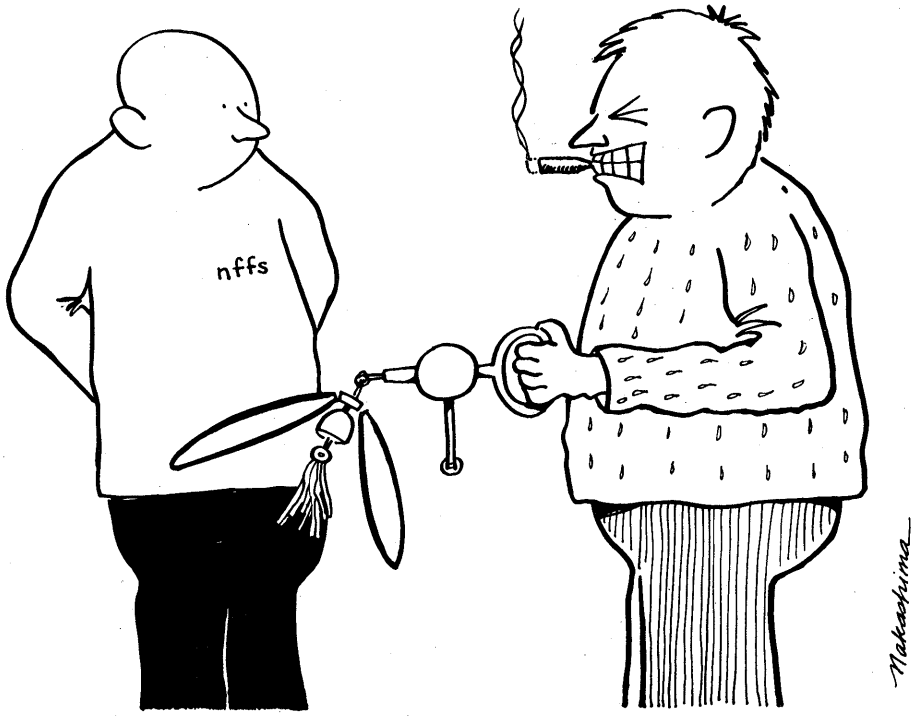

"What happened!? I dropped an ash on the rubber. That's what happened!"